Reversible quasicrystallization in $GeSe_2$ glass

J. E. Griffiths, G. P. Espinosa, J. P. Remeika, and J. C. Phillips
Bell Laboratories, Murray Hill, New Jersey 07974
(Received 13 July 1981)

Absorption of photons at low power levels below the band edge reversibly alters the molecular structure of $GeSe_2$ glass. These structural changes have been analyzed by continuously monitoring the Raman scattering spectrum as a function of time and laser power level. At sufficiently high power levels irreversible crystallization can take place. In the reversible regime four distinct stages of ordering, including a new phenomenon called quasicrystallization, have been observed. Each stage of ordering has been interpreted in terms of rearrangement or joining of molecular clusters which are embedded in the glassy matrix. The relationship between photon-induced cluster reconstruction and photodarkening is discussed. The new phenomena described here demonstrate the inadequacy of chemically ordered continuous-random-network models of chalcogenide glasses and confirm the structural validity of the partially polymerized cluster model.

I. INTRODUCTION

In the absence of long-range crystalline order the direct determination of the atomic structure of glasses by diffraction methods has yielded relatively little information. Thus it is widely believed that the atomic structure of glasses is essentially random, as in random network models of insulating glasses and random packing models of metallic glasses.[1–6]

In recent years it has become apparent that Raman scattering is a powerful probe[7–14] for studying features of the molecular structure of chalcogenide-glass alloys which are not accessible to conventional diffraction techniques. By extending previous Raman studies[7–14] of these alloys we were recently able to show[15] that all the available experimental data are consistent with the notion that a large cluster of atoms is the characteristic structural element of $GeSe_2$ glass. This large cluster was called an outrigger raft. Moreover, it appears at present that no satisfactory alternative to this model is available. Until such an alternative appears, we are heuristically justified in describing the structure of the outrigger raft as well established, and inasmuch as the tentative identification of this structure provided the motivation for the present research, we will leave the philosophical analysis of this situation aside.

The "outrigger raft" is a fragment of the high-temperature form of crystalline $GeSe_2$. We asked ourselves what would become of these partially polymerized molecular fragments if the glass absorbed photons in the Urbach tail region below the Tauc band edge,[16] which is shown schematically[17] for g-$GeSe_2$ in Fig. 1. Studies of the composition dependence of the band edge in Ge_xSe_{1-x} alloys had shown[13] rapid variations with a narrow peak at $x = \frac{1}{3}$, as shown in Fig. 2. This narrow peak is not seen in As_2S_3 or As_2Se_3 glasses. It presumably reflects the stability of $Ge(Se_{1/2})_4$ tetrahedral building blocks.

According to our molecular model a certain concentration of homopolar, i.e., non-chemically-ordered like-atom bonds, is an intrinsic feature of the glass. One might suppose from Fig. 2 that photons absorbed in the Urbach tail would pre-

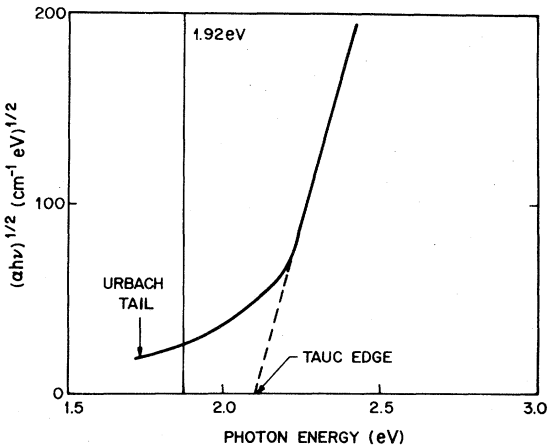

FIG. 1. Absorption spectrum of $GeSe_2$ glass. Experimental data reproduced from Ref. 17 for the reader's convenience.

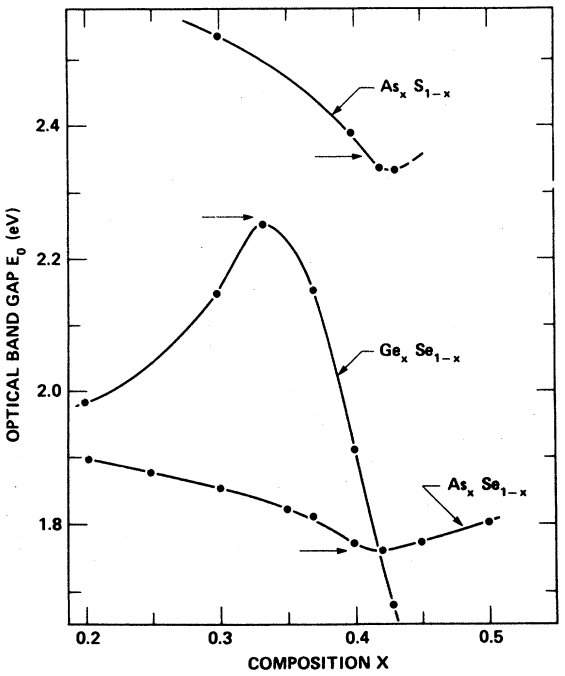

FIG. 2. Composition dependence of the optical-absorption edge in chalcogenide alloy glasses. Data reproduced from Ref. 13 for the reader's convenience.

ferentially break these "wrong" bonds, and that this would be the primary process leading eventually at high power levels to crystallization. More generally other kinds of disorder, e.g., poorly packed and hence strained clusters, would also produce absorption in the Urbach region, which would also contribute to cluster annealing, although on a less localized scale.

Our experimental results are qualitatively in accord with these expectations, but quantitatively we have found that the actual process of laser-induced crystallization is much more complex and sophisticated than we had anticipated. Because of the specific electronic information implicit in the use of Urbach tail photons, we are able to produce structure in the glass which contains many crystalline features in its Raman spectrum but which reverts to the original glassy structure upon elimination of the laser flux. We call this new phenomenon "quasicrystallization." This new phenomenon appears to be essentially athermal and it is associated with an intermediate stage of photodarkening.[18] We also observe several other distinct stages in the development of molecular order in the glassy matrix before irreversible crystallization takes place at high power levels.

The interpretation of the various stages of molecular ordering which we have observed is considerably facilitated if the data are discussed in the context of a specific structural model. Our model is described in detail in Sec. II and is a natural extension of our previous work,[15] which presented a very strong circumstantial case for its validity. More recently chemically specific diffraction data obtained by EXAFS (extended x-ray absorption fine structure) have demonstrated[19] the correctness of the Se-Ge-Se layer model. Direct evidence for broken chemical ordering in $GeSe_2$-$GeTe_2$ pseudobinary alloys has been obtained by measuring electric field gradients by Mössbauer spectroscopy,[20] and the composition dependence of these data has been used to identify the outrigger sites specifically.

II. PARTIALLY POLYMERIZED CLUSTER (PPC) MODEL

Previous workers have shown that the molecular structure of virgin, melt-quenched $GeSe_2$ glass is much more ordered than would be expected from a continuous-random-network (CRN) model. The chalcogenide glass alloys can better be described by small chemically ordered clusters embedded in a continuous network (COCN), according to other Raman-scattering studies.[7–12] Some of these clusters are $(Se)_n$ chains, $Ge(Se_{1/2})_4$ corner-sharing tetrahedra, and $Ge_2(Se_{1/2})_6$ ethanelike structural units, which dominate Ge_xSe_{1-x} alloy molecular structure near $x=0$, $\frac{1}{3}$, and 0.4, respectively.

The strongest Raman-active mode at 202 cm^{-1} in $GeSe_2$ glasses is the A_1 or symmetric breathing mode of $Ge(Se_{1/2})_4$ tetrahedra. This line is quite narrow and its scattering strength is approximately proportional to x for $0 \leq x \leq \frac{1}{3}$, reflecting the replacement of $(Se)_n$ chain segments by $Ge(Se_{1/2})_4$ tetrahedra with increasing x in this interval. Subsequent work based on comparison with the normal modes of vibration of $GeBr_4$ and $GeCl_4$ molecules has led to the identification of all the Raman-active tetrahedral modes in $GeSe_2$ and GeS_2 glasses.[15] The integrated intensity of the 178-cm^{-1} band peaks at $x=0.4$, which led to assigning it[10,12] to the Ge-Ge stretching mode of $Ge_2(Se_{1/2})_6$ units. The very strong and narrow companion A_1 line at 219 cm^{-1} is an edge mode of Se-Se outrigger dimers in the raft model,[15] which assignment is supported by many pieces of evidence[15] including the recent EXAFS[19] and Mössbauer[20] data. The outrigger raft structure is shown in Fig. 3, where it is compared to a section of a crystalline layer.[21]

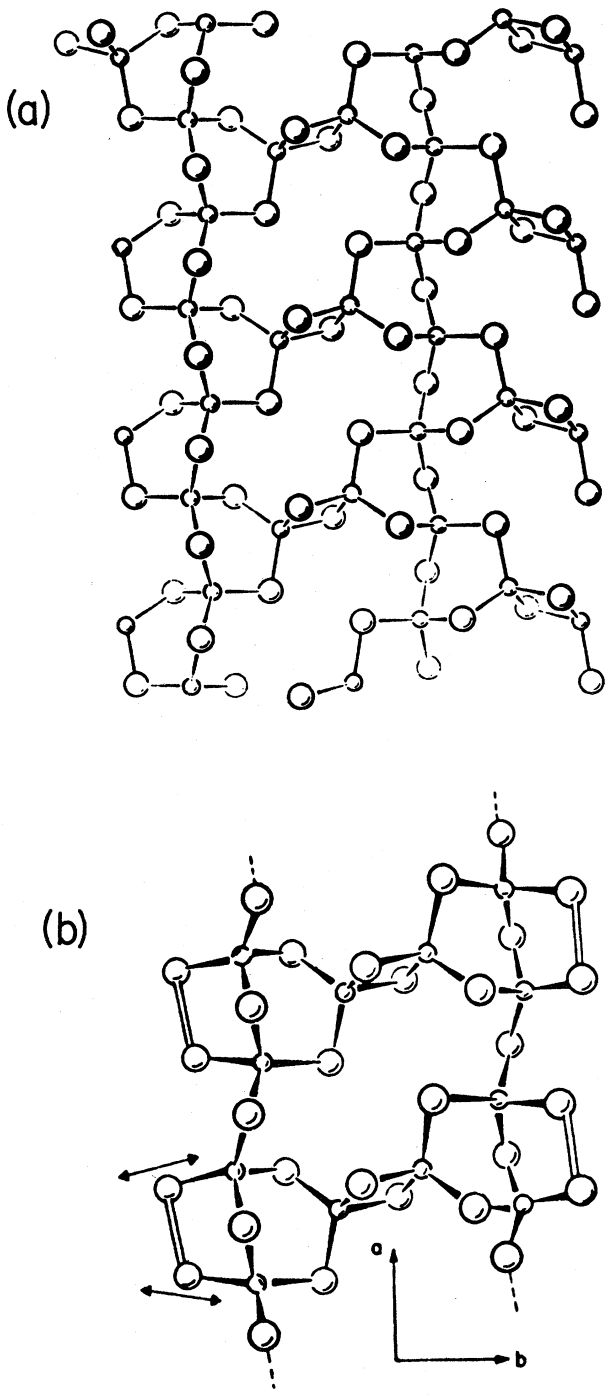

FIG. 3. Molecular models of (a) one layer of the high-temperature form of $GeSe_2$ and (b) the smallest unit of a partially polymerized cluster in the glass. Germanium atoms are represented by the small balls.

An additional feature of the Raman spectrum of the glass which has been observed to vary with laser power level is the Bose-type band at low frequencies below 30 cm^{-1}. We showed by comparison with the spectrum of *c*-$GeSe_2$ that this region is probably associated with interlayer modes of orientationally disordered rafts.[15] These "soft" modes (rafts rotating about their normal axes) are the ones first driven by the annealing effect of the Urbach tail photons.

From these data we have constructed the partially polymerized cluster (PPC) model.[22] According to this model the molecular clusters of *g*-$GeSe_2$ are best described as a strongly associated mixture of large chalcogenide-rich outrigger rafts and small Ge-rich ethanelike units with the proportions adjusted to achieve overall stoichiometry. Both kinds of clusters are locally linearly polymerized and the rafts are locally stacked. This model will be shown to provide a natural explanation for all the stages of Urbach photon-induced molecular reorganization observed in our Raman-scattering data.

III. QUASICRYSTALLIZATION AND MICROCRYSTALLIZATION

There is a clear distinction between a metastable $GeSe_2$ glass and a thermodynamically stable crystal of $GeSe_2$. In the context of the PPC model, outrigger rafts of variable lateral (*a* and *b*) dimension, characterized by the topological repeat parameters *m* and *n*, tend toward layered structures in the glass phase. Layering is stabilized by weak inter-raft van der Waals forces. The individual rafts have short- and intermediate-range order in the *a* and *b* directions but lack the *three-dimensional* long-range periodicity characteristic of the crystalline phase.

Between these extremes is the quasicrystalline material, which is a different type of ensemble that can result from photon-induced cluster growth in the lateral directions. With an increase in intermediate-range order that such growth implies, several changes in the Raman spectrum are anticipated. Increased ordering should cause narrowing and possibly shifting of the peak Raman frequencies of the major intramolecular bands. Because quasicrystallization occurs *after* a drastic change in the number density of cluster-defining Se—Se and Ge—Ge bonds, the intensities of the bands at 219 and 178 cm^{-1} representing motions of these specific atom homopairs should decrease or disappear entirely. Furthermore, as some of the clusters reach a sufficient size to support quasilattice modes, the bands at low frequency should either narrow or new sharper bands should grow at their expense. True lattice modes whose frequencies,

bandwidths, and relative intensities *all* agree with those of the crystal cannot appear until a three-dimensional lattice develops.

There is, at present, no criterion established that defines the minimum three-dimensional crystallite size necessary to have the same lattice-dynamic properties as a macroscopic crystal. One might reasonably expect, however, that a crystallite containing several units cells would be required. For some materials, crystallites of 15 to 30 Å are adequate.[23] The same is probably true of a quasicrystallite. The major difference between the two structures may be the lack of ordering perpendicular to the cluster planes and the lack of a completely ordered arrangement of atoms in the planes. This would have the effect of producing broader bands for the quasicrystal, even through the Raman frequencies correspond closely to those of a true crystal.

A mechanism initiating and propagating the formation of quasicrystalline $GeSe_2$ follows directly from the PPC model and can be photon induced or thermally assisted or both. The first step, light-induced photodarkening,[14,18,24,25] is not model specific. It caused an increase in the absorption coefficient of the material in, and just above, the Urbach tail. Cluster reorientation and reassociation at this stage may ease the energy burden of ultimately breaking like-atom Ge—Ge and Se—Se bonds. This is equivalent to saying that the absorption edge, or Tauc edge as shown in Fig. 1, moves to lower energy as photodarkening occurs. The effect is to increase temporarily the level of the Urbach tail at the irradiation energy, in this case 1.916 eV. It will be shown later that at this stage the photodarkening process is delocalized over the complete glass structure and does not arise from the cleavage of specific bonds.

Following initial photodarkening, further increasing the photon flux can lead to the breaking of edge Se—Se and Ge—Ge bonds. Our data suggest that the outrigger rafts grow laterally, thereby reducing the concentration of Ge-rich ethanelike clusters and Se-Se-raft terminating ring structures.

This lateral growth or quasicrystallization occurs at the cost of leaving the ensemble of larger clusters which are still embedded in and partially polymerized to the glassy substrate under considerable strain. Removing the photon flux promotes strain memory-driven relaxation of the system toward the original structure. Increasing the photon flux will allow quasicrystallization to propagate until rearrangement of quasicrystallites by reorientation about the quasi c axis and translation along a and/or b axes allows microcrystallization to occur. During this major reorganization of the structure, development of strain can be substantial if microcrystallization does not dominate the irradiated volume element of the sample. Under such conditions, removal of the photon flux may still allow reversibility of the complete process. Reversibility of microcrystallization would not normally be anticipated on macroscopic equilibrium thermodynamic grounds, but evidence for it will be presented in subsequent sections.

IV. EXPERIMENTAL PART

A. Preparation of glasses

In a typical preparation, powdered germanium (99.999% pure) and previously vacuum melted selenium (99.999% pure) were weighted in a 1:2 mole ratio and sealed under vacuum in a 6 cm fused silica tube (6 mm i.d.). The mixture was heated at 905 °C for 3 h with intermittent rocking of the sample tube to ensure complete mixing before quenching directly from the furnace into water. A clear red glass resulted which lacked any discernible x-ray crystal powder pattern.

Samples whose stoichiometry varied from $GeSe_{1.849}$ to $GeSe_{2.249}$ were characterized by their differential thermal analysis (DTA) patterns. About 0.071 $\pm$0.0005 g samples of small unground glass pieces were placed in the holder of a Model 990 Dupont thermal analysis instrument fitted with a high-temperature 1600 °C DTA cell and heated at a constant rate of 10 °C per min under argon. Characteristic values were obtained for the glass transition temperatures T_g,[26] the crystallization temperatures T_c, and the temperatures at which one or two small endotherms appeared above the crystallization temperature. These endotherms as well as T_c were stoichiometry dependent. The highest of the two endotherms near $T_{x2}=582\pm2$ °C correlates very well with the melting temperature of the eutectic between GeSe and $GeSe_2$.[27] It appears for all samples having Se-to-Ge ratio less than 2.0. The first endotherm near $T_{x1}=575\pm2$ °C may be due to a phase transformation[27,28] in the minute amounts of GeSe present in the germanium-rich samples. To prevent rupture of the fused silica tubes during heating at high temperatures and the attendant risk of exposure to toxic selenium vapors, no sample tubes were com-

pletely filled with Ge and Se. The vapor above the liquid is likely to be richer in selenium than the liquid, which makes it extremely difficult to prepare glasses having a precise Se-to-Ge ratio equal to 2.00. Values of T_c as a function of nominal composition peak at this ratio.

B. Raman experiments

Irregularly shaped glass samples were about 3×3 mm^2 and about 0.5 to 1 mm thick. A sample was mounted on the copper cold finger of a liquid nitrogen Air Products cryostat via thermal grease (Air Products) such that the external curved surface shaped by the original quartz tube was presented to the incoming laser beam. The beam entered the sample at about 70° to the surface normal and scattered light was collected at 90° to the incident beam. The electric vector of the laser beam was either in the plane of incidence (H) or perpendicular (V) to it.

Raman excitation was done using the 6471 Å line of a Spectra Physics Model 164 krypton-ion laser. Most experiments utilized H polarization so that penetration of the beam into the sample was favored over reflection. Scattered light was analyzed using an Instruments S. A. Ramanor HG-2S spectrometer and detected with a Hammamatsu 928 photomultiplier and associated photon counting electronics. A Data General Eclipse S-130 minicomputer controlled all aspects of the apparatus and the experiments. Typical parameters were stepping increment 0.2 cm^{-1}, counting time 1.0 sec, spectral slit width 3.0 cm^{-1}, and cryostat tip temperature -196 °C. Laser power at the sample varied from about 2 to 100 mW as measured with a calibrated Model 460 power meter. Using a modestly focused beam, the photon flux at the sample covered the range 6×10^{15} to 3×10^{17} photons cm^{-2}sec^{-1}. With such relatively high photon fluxes entering an absorbing medium, it was prudent to do all Raman experiments with samples heat sunk to a massive copper tip at -196 °C. Under such conditions, the sample temperature, as measured by anti-Stokes–Stokes ratios, would rise but not above room temperature and certainly would not reach the glass transition or crystallization temperature. Bonding and structural changes could then be attributed to optical and not thermal effects with reasonable confidence.

V. RESULTS AND DISCUSSION

A. Sample characterization

All $GeSe_x$ samples ($1.849 \leq x \leq 2.249$) were characterized by their glass transition temperatures $T_g \sim 392$ °C, which were fairly constant, their crystallization temperatures T_c, which were not, and by the presence or absence of one or two small endotherms at $T > T_c$ which occur for Se-to-Ge ratio less than 2.00. Typical DTA patterns are shown in Fig. 4. Figure 5 is a plot of T_c as a function of nominal composition. It demonstrates the high sensitivity of T_c to extremely small variation in the Se-to-Ge ratio. Only two of ten attempts to prepare samples with Se-to-Ge ratio exactly at 2.00 ($T_c = 533$ °C) were successful. The rest had T_c values between 512 and 517 °C corresponding to Se-to-Ge ratios between 1.992 and 1.995. The origin of the endotherm [Fig. 4(a)] at $T_{x1} = 575$ °C is unknown. The endotherm has been observed earlier[27,28] and it appears only over a limited composition range near $GeSe_2$. For this reason it is not likely to be due to a phase transition in the minute amounts of GeSe that may be present. It is more likely to arise from solid solubility of GeSe in $GeSe_2$.

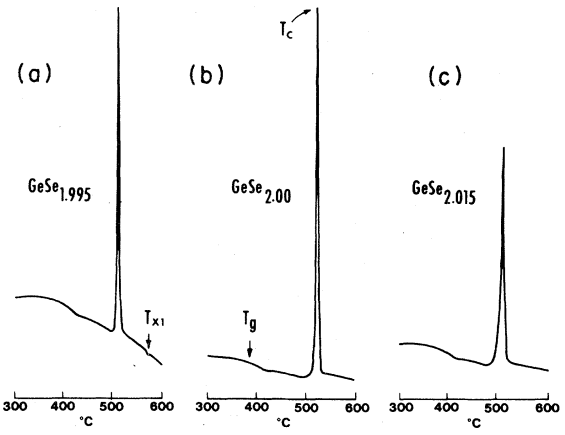

FIG. 4. DTA patterns for $GeSe_{1.995}$, $GeSe_{2.00}$, and $GeSe_{2.015}$. T_{x1} is the first endotherm, T_g is the glass transition temperature, and T_c is the crystallization temperature.

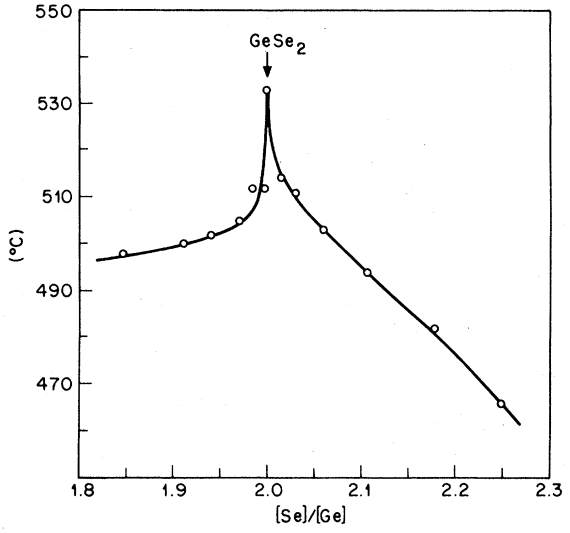

FIG. 5. Variation of T_c as a function of the Se-to-Ge ratio near the stoichiometric composition Se-to-Ge ratio equal to 2.000.

All the samples used for Raman scattering had compositions in the range $1.995 < \text{Se/Ge} < 2.015$. Determining such small variations in composition is beyond the limits of reliability of normal analytical techniques. Thus the DTA method of characterizing our samples is the best that can be done. In any case, the Raman scattering results are not especially sensitive to these very small composition variations as is evident from Fig. 6.

B. Photodarkening

Figure 7 shows that photodarkening initially occurs without selective bond breaking within a cluster. The peak intensities of the Raman bands centered near 20 cm^{-1} (Bose peak), 178 cm^{-1} ($Se_3Ge-GeSe_3$ wrong bond stretching vibration), 201 cm^{-1} (symmetrical stretching of $GeSe_4$ linked tetrahedral), and 218 cm^{-1} (companion line involving motion of the Se-Se cluster terminating linkage) are plotted against laser power at the sample. Each data set shows a similar power dependence differing only in the magnitude of the signals. If bond breaking or bond rearrangements were involved, the shapes of the individual curves would differ significantly.

At low powers ($P < 20$ mW) the peak intensities linearly as expected for a material whose absorption coefficient is only weakly dependent on incident power. The effects of absorption become increasingly important at $P > 20$ mW. As the absorption edge moves toward the wavelength of the exciting light (see Fig. 2) the peak intensities of all of the bands begin to decrease, falling about a factor of 100 at $P = 70$ mW compared to the values expected from extrapolations of low power data. At power levels above 70 mW dramatic changes occur in peak frequencies, band centers, and in peak intensities. These changes are produced by photoinduced bond breaking and reformation.

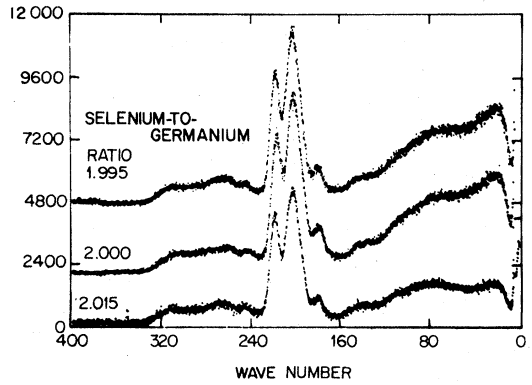

FIG. 6. Raman spectra of $GeSe_2$ glasses with Se-to-Ge ratio of (top) 1.995, $T_c = 512$ °C, $P_0 = 16$ mW; (middle) 2.00, $T_c = 517$ °C, $P_0 = 20$ mW; (bottom) 2.015, $T_c = 514$ °C, $P_0 = 24$ mW. Sample temperature, −196 °C. Spectra are vertically offset for clarity.

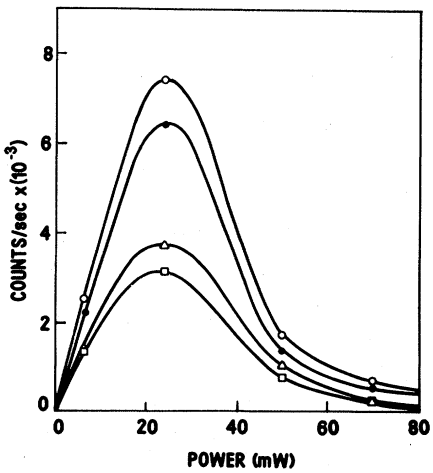

FIG. 7. Photodarkening in $GeSe_2$ glass. Raman signal amplitude (C/S) vs laser power (6471 Å) at the sample ○ = 202 cm^{-1} (● = 219 cm^{-1}, Δ = 20 cm^{-1}, □ = 178 cm^{-1}).

C. Raman spectra

Valence force-field calculations and vibrational assignments of bands to symmetry coordinates for Ge_xSe_{1-x} glasses are well documented.[9–15] Spectra of samples having minor composition differences ($1.99 \leq Se/Ge \leq 2.015$) were shown in Fig. 6 to demonstrate their near vibrational equivalence. The one exception is the apparent shape of the low-frequency Bose peak. The bottom spectrum in Fig. 6 has less low-frequency scattering in general due in part to a smoother external surface, to a lower vibrational temperature, and more photodarkening for this sample compared with the other two.

Figure 8 shows the effect of laser power on a single sample having Se-to-Ge ratio equal to 2.015 ($T_c = 514$ °C). This was chosen because at this composition there is no evidence for any melting of material at the eutectic composition and thus no GeSe discernible in the glass. Each spectrum of Fig. 8 is offset from zero for clarity and normalized at the $Ge(Se_{1/2})_4$ 202-cm^{-1} band so that signals will have comparable amplitudes. Incident laser power increases from *A* through *D* and decreases for *E* and *F*. The changes that occur are discussed by focusing on various spectral regions.

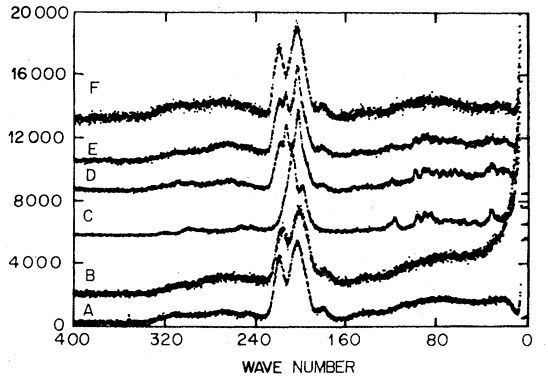

FIG. 8. Raman spectra of $GeSe_{2.015}$ at −196 °C. Stepping increment 0.2 cm^{-1}, counting time 0.5 sec, and spectral slit width 3.0 cm^{-1}. Spectra are offset for clarity and intensity normalized at $\Delta\nu = 202$ cm^{-1} by a scaling factor marked as *xn*. Laser power in mW (6471 Å) at the sample are *A*, 24; *B*, 50; *C*,84; *D*,20; *E*,20; *F*,20. Sample *E* was allowed to relax in the dark at room temperature for 17 h before cooling to −196 °C and recording spectrum *F*. *D* was relaxed in the dark at room temperature for 45 min before cooling to −196 °C and recording spectrum *E*.

D. Intramolecular 160–260 cm^{-1} region

This spectral region is shown in expanded form in Figs. 9–11 to demonstrate the dramatic changes that occur as a function of incident laser power. Figure 9 (*A*–*C*) with laser-power values of 24, 50, and 84 mW show several effects. From *A* to *B* there is a decrease in signal amplitudes corresponding to photodarkening, a minor shift (~1 cm^{-1}) to lower values for the Se-Se 219- and Ge-Ge 178-cm^{-1} peaks, and a noticeable broadening of both the 219- and 178-cm^{-1} bands. More drastic changes occur between *B* and *C* where the wrong-bond 219- and 178-cm^{-1} bands disappear. The $Ge(Se_{1/2})_4$ 202-cm^{-1} band is still evident but has shifted to 199 cm^{-1}. A new band at about 207 cm^{-1} has appeared and is assigned in our model to the symmetric stretching modes of the quasicrystalline $Ge(Se_{1/2})_4$ tetrahedra. Reducing the power to 20 mW as opposed to cutting off the photon flux entirely allows continued growth and rearrangement of the quasicrystallites until in Fig. 10 (curve *D*) some microcrystallites have appeared in the matrix of glass. This is evident from the appearance of the band at $\Delta\nu = 210.7$ cm^{-1} (single-crystal value 210.3 cm^{-1}). The development of microcrystallite bands is accompanied surprisingly by the *reappearance* of the glass bands at 281, 202, and 178 cm^{-1}. Removing the photon flux and allowing the temperature of the sample to rise to room temperature during 45 min prior to recooling to −196 °C and reimposing 20 mW of laser power on the sample results in Fig. 10 (curve *E*). The trend towards microcrystallization has been partially reversed as evidenced by a decrease in the intensity at 210.7 cm^{-1} relative to the peaks due to the glass. Figure 11 (curve *F*) is the spec-

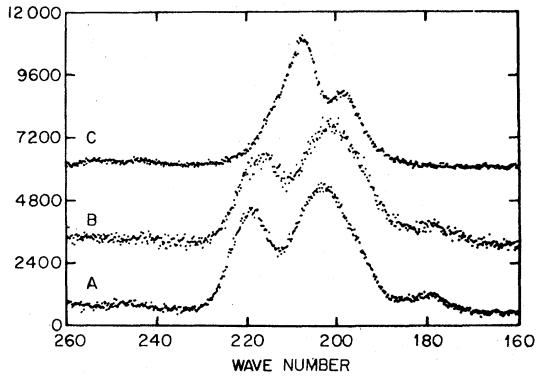

FIG. 9. Expanded-scale Raman spectra of $GeSe_{2.015}$ at −196 °C from Fig. 8.

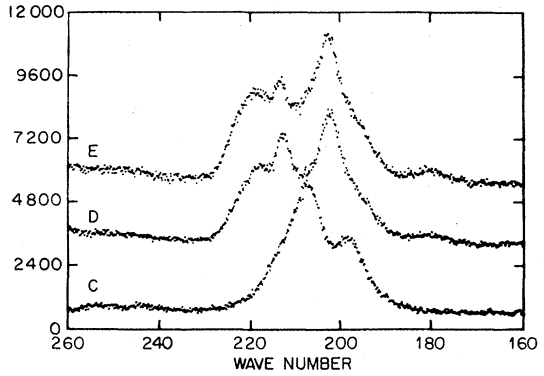

FIG. 10. Expanded-scale Raman spectra of $GeSe_{2.015}$ at −196 °C from Fig. 8.

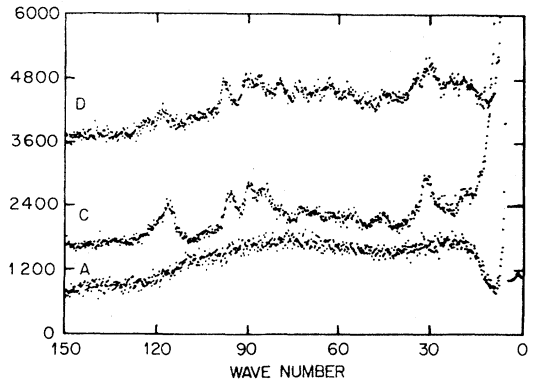

FIG. 12. Expanded-scale Raman spectra of $GeSe_{2.015}$ at −196 °C from Fig. 8.

trum of the sample after relaxation overnight in the dark at room temperature. It is indistinguishable from the initial glass spectrum of Figs. 8 (curve *A*), 9 (curve *A*), and 11 (curve *A*). The spectrum of Fig. 10 (curve *D*) is repeated for the reader's convenience in Fig. 11 (curve *D*).

E. The low-frequency region

This part of the spectrum is more difficult to assign in terms of symmetry coordinates. The observed effects, however, are no less dramatic and contain significant information. Low-frequency spectra selected for Fig. 12 include *A*, the low-power 24-mW spectrum; *C*, the 84-mW spectrum corresponding to the noticeable appearance of the quasicrystalline phase; and *D*, the spectrum of the sample containing microcrystallites and glass. *C* shows the appearance of quasicrystalline lattice modes. Some but not all of the lattice modes expected for crystalline material are observed, the most notable absentees being the 61- and 72-cm^{-1} bands. (It would be interesting to identify these normal modes in a molecular model.) In *D*, the lattice modes and broad glass spectral features mask each other so that only the major features of both are discernible.

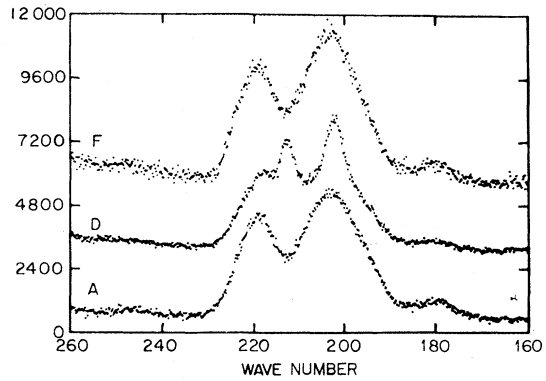

FIG. 11. Expanded-scale Raman spectra of $GeSe_{2.015}$ at −196 °C from Fig. 8.

The main points are the reversibility of the process as a function of photon flux and time and the fact that a clear distinction between the crystalline phase, the glass phase, and the intermediate quasicrystalline phase can be detected in the vibrational Raman spectra. It is important to note the *simultaneous* disappearance of the Se-Se companion line at 218 cm^{-1} and the ($Se_3Ge-GeSe_3$) mode at 178 cm^{-1}, the appearance of a new mode at 207 cm^{-1}, and the emergence of latticelike modes corresponding to the formation of the quasicrystalline structural units in the sample. Furthermore, reversibility is not suppressed by the appearance of lattice modes. This occurs readily and reproducibly on complete removal of the proton flux after formation of quasicrystallites.

F. Effect of annealing

A piece of the same sample Se-to-Ge-ratio equal to 2.015 was annealed in vacuum at 415 °C ($T_g \sim 382$ °C, $T_c = 514$ °C) for 3 h prior to a series of Raman experiments. Microscopic examination of the outside surface of the sample that had been in contact with the sealed fused silica tube during annealing revealed the presence of a few patches of dendritic crystalline selenium.[29] Dendrites were about 20−30 μm long. The inside surface was free of these crystals and this part of the sample was used for Raman experiments. As before, a typical

glass spectrum was observed at low power (40 mW). At power levels of more than 80 mW, well-developed crystallite spectra were recorded. In this case, the lattice modes were much more dominant. Figure 13 shows such a comparison for three regions of the spectrum. The top spectrum in each region is the low-power (40 mW) spectrum and the corresponding lower spectrum in each box is that resulting from exposure of the sample to a 100-mW laser beam. In each panel the difference is striking and this is especially true in the lattice mode region below 120 cm^{-1} and in that above 240 cm^{-1}. In annealed samples, it is more difficult to arrest the reorganization of the glass at the quasicrystallite stage. It has been done, however, by a gradual increase of laser power with continuous monitoring of the Raman spectra.

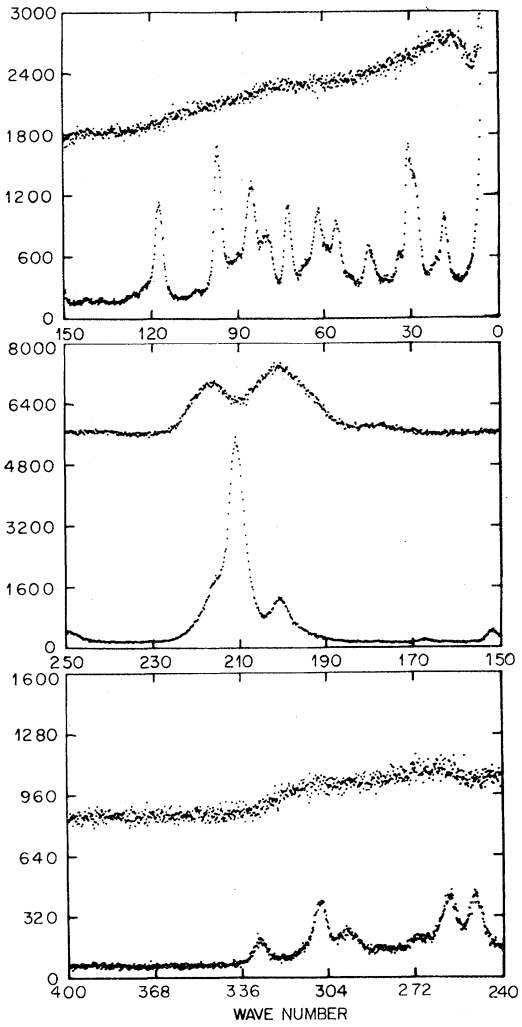

FIG. 13. Comparison Raman spectra of annealed (415 °C/3 h) $GeSe_{2.015}$ at −196 °C (bottom of each frame) of sample phototransformed using 100 mW (6471 Å) to obtain microcrystallites of $GeSe_2$ and (top of each frame) of sample relaxed in the dark at room temperature to reversibly transform the sample to a glass. Note the presence of the narrow crystalline line at 211 cm^{-1} and the glass lines at 216 and 202 cm^{-1} in the middle frame (lower spectrum) and the lack of crystallites in the upper spectrum after relaxation in the dark.

That the sample represented by Fig. 13 (bottom) contains microcrystallites after the above treatment and not quasicrystallites, is demonstrated clearly in Fig. 14 where a comparison is made between the sample containing microcrystallites and the spectrum of a single crystal of $GeSe_2$. From 150 to 400 cm^{-1}, all of the previously reported[15] crystalline Raman bands appear in the spectrum of the transformed annealed glass sample. Between 0 and 150 cm^{-1} there is general agreement in the number and the frequencies. Some anomalies exist in the relative intensities and in the number of lattice modes present. There are more in the transformed glass. This is readily understood by considering the spatial orientation of microcrystallites in the transformed glass. The bottom spectrum (single crystal) is a polarization analyzed (*HH*) spectrum of the single crystal oriented in a particular direction in a laboratory axis system. Rotating the crystal 90° about the *c* axis of Fig. 3(a) and measuring *HH* and *HV* spectra for each orientation yields four spectra in which the wave numbers and relative intensities of the lattice modes change significantly (Fig. 15). (For completeness the frequencies of all lattice modes are tabulated in Table I.)

A weighted average of the intensities of these spectra reproduces all of the lattice modes of the transformed glass of Figs. 13 and 14. It would appear, therefore, that the microcrystallites in the transformed glass sample are orientationally disordered. Lacking spectra of the crystalline sample in which the electric vector of the laser beam oscillates exactly along the *a* or *b* axis of Fig. 3(a) makes it impossible to analyze the data further. It is of interest, however, to note that the sample discussed above, in which microcrystallites are well formed, reverts to an all-glass state indistinguishable from a freshly quenched sample. As expected, reversibility is not fast, even at more elevated temperatures (−60 °C/3 h), suggesting a strain-driven molecular rearrangement process in an extremely high viscosity system.

The photoinduced evolution of the structural reorganization occurring within the $GeSe_2$ glass is summarized in Table II. Raman data from 0 to

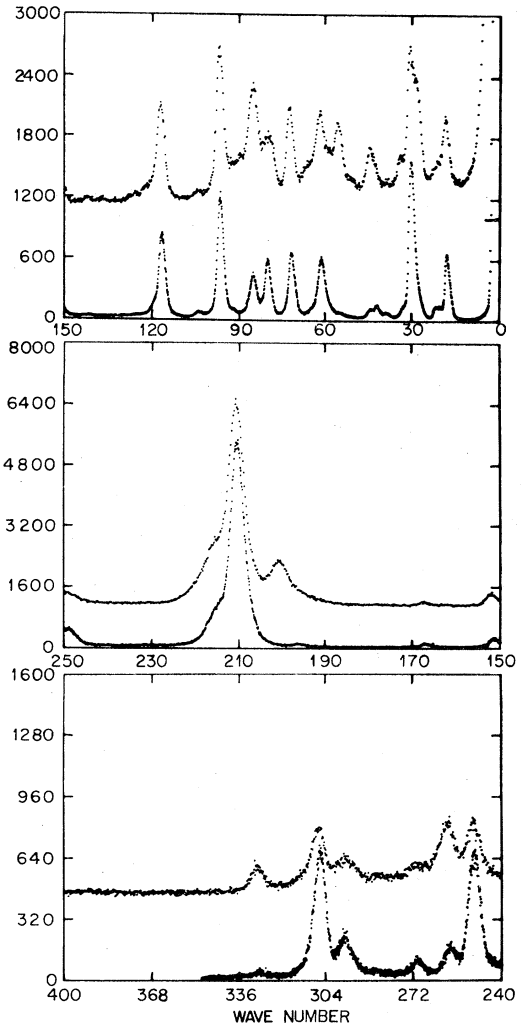

FIG. 14. Comparison of Raman spectra of annealed (415 °C/3h) $GeSe_{2.015}$ at −196 °C (top of each frame) of sample phototransformed using 100 mW (6471 Å) to obtain microcrystallites of $GeSe_2$ and (bottom of each frame) of a single crystal of $GeSe_2$. Experimental variables are the same as Fig. 13 for the top spectra. For single-crystal spectra, stepping increment 0.1 cm^{-1}, counting time 0.5 cm^{-1}, spectral slit width 1.5 cm^{-1}, polarization *HH*.

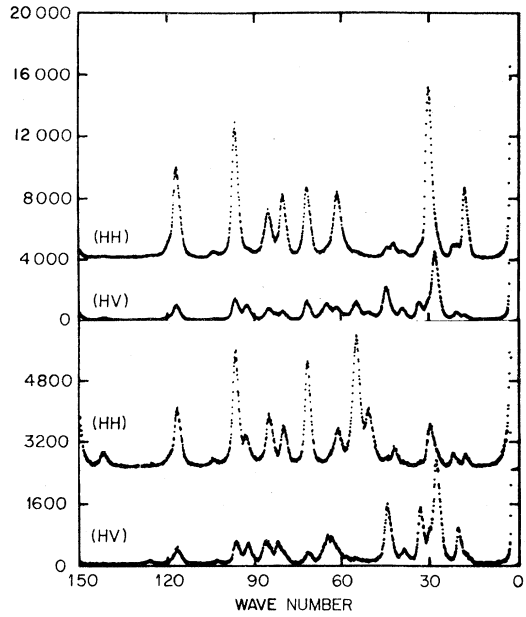

FIG. 15. Polarization spectra (*HH* and *HV*) of single-crystal $GeSe_2$. Top two and bottom two spectra differ by sample rotation of 90° about the *c* axis. The orientation of the *a* and *b* axes in the laboratory frame of reference is unknown. Experimental variables are the same as Fig. 14. Laser power (6471 Å) is 30 mW.

120 cm^{-1} are listed in terms of the dominant morphology present in the scattering region of the sample. The appearance of the prominent bands at 62, 72, and 80 cm^{-1} in columns 3 and 4 signal the formation of a true crystalline phase. At this point, the photoinduced laterally growing quasicrystalline units have become sufficiently large and spatially well oriented to allow long-range atomic periodicity to occur.

In order to obtain reproducible results we have performed almost all our experiments on melt-quenched bulk samples. In a few runs on evaporated films (thicknesses near 1000 Å) we were unable to observe reversible behavior. In the absorption depth sampled by our photons (which decreases with increasing power level and increasing photodarkening), we have observed reversible behavior even when the Raman spectrum is 80% microcrystalline. It is important, however, to bear in mind that in each stage as the transformation proceeds in the bulk sample the transforming region consists of strata which are sequentially and integrally superimposed on lower layers which remain in less transformed states. Thus the succeeding strata and finally the virgin substrate act as laterally homogeneous reference structures toward which the microcrystallized regions will thermally relax when the pump photons are removed. We may even go so far as to conjecture that irreversible crystallization occurs in the surface region when grain boundaries appear between surface microcrystallites to interrupt the lateral homogeneity of this region. On the other hand, in thin films reversible behavior may not be observed for several reasons, e.g., mechanical substrate

TABLE I. Raman spectra of $GeSe_2$: single crystal, photocrystallized glass, and melt-quenched glass. Frequency shifts (ν) and intensities (c/s) are given in cm^{-1} and counts/sec, respectively.

Crystalline $GeSe_2$[a]								Photo-crystallized glass		Melt-quenched glass[b,c]	
HH(1)		*HV*(1)		*HH*(2)		*HV*(2)					
ν	c/s	ν	c/s	ν	c/s	ν	c/s	ν	c/s	ν	c/s
17.7	4710	17.7	436	17.3	360	17.2	310	17.7	1000		
20.3	1000					19.9	960				
21.5	1020	20.4	575	21.5	400			20.9	586	20	weak
		27.9	4540			27.3	2710	27.8	1370		
30.0	11 230			29.3	1160	30.0	900	30.1	1680		
33.1	850	33.3	1220			32.8	1540	33.4	630		
38.6	510	38.9	900	38.8	220	38.6	400	38.5	400		
41.9	1000			41.5	550						
44.1	770	44.5	2220			44.1	1590	44.4	700		
		50.6	600	50.5	1570			50	50		
55.0	545	54.7	1270	54.7	3460	55.3	180	55.8	960		
						58.4	250				
61.2	4290	61.4	900	61.1	1050			61.5	1060		
		64.9	1130			64.2	750	65.5	570		
71.5	4780	71.7	1240	71.5	2780	71.3	320	72.5	1090		
80.0	4340	80.2	670	80.0	1110	81	600	80.1	845	82	weak
85.1	3250	84.9	795	84.8	1400	85.8	615	84.9	615		
92.0	725	92.5	1030	92.8	820	92.2	575	90.0	640		
96.7	8730	96.6	1410	96.6	3060	96.5	620	96.8	1700		
104.0	515	103.3	155	104.4	250	103.1	120	104.2	260		
116.9	6000	116.8	1050	116.7	1620	116.7	400	117.3	1130		
119.6	1100							122.1	310		
		125.7	115			126.1	105	126.0	250		
								137.2	180		
141.9	300	141.9	210	141.9	425			142.5	180	145	weak
151.2	890	151.3	800	151.1	2200	151.1	100	151.8	440		
166.6	280	166.9	350			166.7	470	167.3	210		
195.9	320	196.1	180	195.4	190	195.5	90			178	weak
								200.5	1290	202	strong
210.4	18 600	210.3	6000	210.3	12 770	210.3	1450	210.7	5550		
215.5	3000	215.1	1300	215	2400	216.1	300	216.0	1700		
										219	strong
230.9	260			232.0	170						
249.5	1550	249.5	230	249.3	380	249.4	250	249.6	430	248	weak
258.6	400	258.7	480	259.2	700	259.2	75	258.9	430		
270.2	170	270.5	230	270.5	90	270.0	250	270.8	210	269	weak
		285.3	50	283.5	80	284.8	50	284.9	160		
296.7	520	296.6	120	296.2	130	297.3	80	296.6	250		
305.9	1600			305.8	550	307.0	200	306.7	400		
				313.9	100					315	weak
329.1	110			328.9	920	329.2	40	329.5	200		
						336.0	40				

[a]Samples (1) and (2) differ only in a sample rotation of 90° about the *c* axis (Fig. 3). Laser penetration and polarization directions are near parallel to the *c* axis and almost parallel to the *ab* crystal plane, respectively.

[b]Because of the large differences in absorptive properties of the crystal and the glass and the much greater breadth of the glass bands, only a qualitative measure of the glass intensities is given.

[c]Tentative assignments were given in Ref. 15.

TABLE II. Low-frequency Raman spectra of $GeSe_2$: *A*, glass; *B*, quasicrystalline and glass; *C*, microcrystalline and glass; and *D*, mostly crystalline. Numerical data in cm^{-1}.

A: Glass	*B*: Glass and quasicrystalline	*C*: Glass and microcrystalline	*D*: Mostly microcrystalline
			17.7[c]
	19	20	
20[a]			20.9
		24	27.8
	31	31	30.1
		35	33.4
			38.5
	46	45	44.4
			50
		57	55.8
		62	61.5
			65.5
		73	72.5
82[b]		80	80.1
	85	87	84.9
	90	91	90.0
	96	98	96.8
			104.2
	116	118	117.3

[a]Bose peak (very broad).
[b]Intramolecular tetrahedral deformation mode.
[c]Earlier assignments in Ref. 5.

clamping or the absence of a virgin glass reference substructure, as in the bulk case.

Another feature which distinguishes the microcrystallite morphology from the quasicrystalline morphology is that the Urbach tail in the absorption edge of the former is expected to be much weaker than for the latter, i.e., the photodarkening trend is reversed by the quasicrystallite→microcrystallite transformation; stage *C* to stage *D*. If this transformation primarily affects the surface stratum, then initially it will increase the absorption depth and the light will penetrate to the glass stratum which lies below. This explains the surprising *reappearance* of the 218-, 202-, and 178-cm^{-1} glass bands in stage *D* which was mentioned above. Of course, with further exposure the interface between the transformed and untransformed region moves deeper into the glass and eventually the glass bands disappear.

A general feature of our observations is that formation of a given morphology (say microcrystalline) requires a high power level (say 100 mW or greater), but that growth of this morphology, once formed, can be sustained at a much lower power level (say 20 mW). The growth, of course, represents a movement of the lower interface of the stratum further into the sample, so that the entire photoinduced process is similar to conventional crystal nucleation and growth. One could investigate the power level at which a given interface is stationary against the effective pressure of thermal disorder of the substrate. This stationary power level would be a function of both temperature and morphology.

There is one additional point to be made. There have been close to a dozen experimental Raman-scattering studies of $GeSe_2$, and in none of them was evidence for quasicrystallization, microcrystallization, or reversibility reported. The reason is quite obvious when one considers the laser-excitation wavelengths used and the optical absorptive properties of the sample. With the exception of the present work, which was done using the 6471 Å (1.916 eV) krypton-ion laser line, other work was done with either 7525 Å (1.648 eV) or 7933 Å (1.551 eV) laser excitation. Even with pho-

todarkening, which was not reported, these low-flux excitations (Fig. 2) are so far from the absorption edge that not enough energy would have been available to initiate quasicrystallization. In all of the earlier work, great care was taken to ensure that the effect of laser irradiation on the sample was minimal. In the present work, advantage was taken of photoinduced reconstruction to probe more effectively the details of the structure of $GeSe_2$ glass.

VI. CONCLUSIONS

The photon-induced transformation from glass to partial microcrystallization has been studied in detail and has been shown to be fully reversible. An intermediate stage, quasicrystallization, has been identified in which large clusters are formed with narrow Raman bands. These clusters lack some of the Raman lines associated with microcrystallites. Their stability range can be narrowed by thermal annealing prior to photoexposure. The structure of quasicrystallites is a challenging problem for future study.

Our entire interpretation is based on the replacement of wrong bonds by right bonds through selective photon absorption. In our model wrong bonds are an intrinsic feature of the melt-quenched stoichiometric glass. The difference between our PPC (partially polymerized cluster) model and the chemically ordered continuous network model (COCN) model is illustrated in Fig. 16. In our model the number of wrong bonds at the stoichiometric composition is not zero (as in the COCN) but it is much smaller than in the continuous random network model (CRN). The wrong bonds arise in a fundamental sense because the glass transition takes place at $T = T_g > 0$. Hence there must be not only configurational disorder but also some degree of chemical disorder. This chemical disorder is exploitable through selective photon absorption because of the narrow peak in the band-edge absorption-edge energy at the stoichiometric composition shown in Fig. 2.

A general feature of the present results is that molecular reorientation and reconstruction takes place in successive stages rather than as one continuous process. (Similar transformational sequences have been observed in metastable metallic glass microphases prepared by splat quenching.[30]) The partially polymerized clusters which are present in the glass can be regarded as one stage of

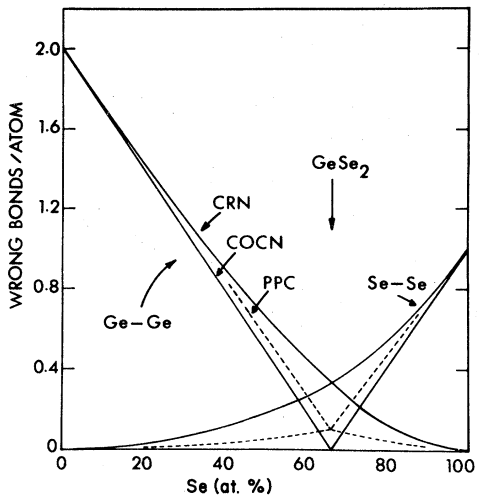

FIG. 16. Homopolar wrong-bond counting statistics in $GeSe_2$ glass CRN is a completely random network model; COCN is a chemically ordered covalent network model, and PPC is a partially polymerized cluster model.

the ordering process. It has been shown, however, that the first sharp diffraction peak is present[31] in liquid $GeSe_2$ for $T > T_m$. This means that short of vaporizing the material there is always substantial order not envisioned in random network models. It is this substantial order which we have shown can be reversibly tuned over a wide range.

In the absence of specific evidence to the contrary, scientists often assume that the microstructure of a condensed material can adequately be described in macroscopic terms as either liquid, crystalline, or, for special materials, glassy. Typically, the preferred evidence is obtained from diffraction experiments which routinely identify crystalline microstructure on a scale of 100 Å or more. Because of the small volume transformed by laser annealing in our samples, x-ray diffraction is not appropriate, and because of the sensitivity of the glass to molecular damage we have not attempted diffraction experiments by reflection-electron microscopy. This apparently leaves open the possibility that the crystallization effects that we have observed are merely thermal, and that they arise from macroscopic melting of the sample surface layer by fluctuations in the laser beam at higher power levels.

We believe that a careful study of the transformational sequences reported here will convince the reader that macroscopic melting is not an adequate explanation for the effects we have observed. For the more hurried reader we offer the following ad-

ditional comments. The melting point $T_m(GeSe_2)$ and the boiling point $T_b(Se)$ are both close to 1000 K. If the sample indeed melted, the vapor pressure of Se would be high. Crystallization from the melt of a glass-forming material requires times of order 1 min, and during this time substantial quantities of Se should evaporate from the sample surface, leaving behind a residue of microcrystalline GeSe (which is not a glass-former). As little as a few percent *c*-GeSe would easily be identified in our Raman spectra, but during several reversible transformation sequences none has ever been observed. This is a strong argument against macroscopic melting.

Another reason for doubting that macroscopic melting can have taken place lies in the dramatic and novel reversibility of the transformation sequence. The postulated fluctuations in laser intensity must take place on a lateral scale of at least 10^{-4} cm and more probably on a scale of order 10^{-2} cm or larger. It is difficult to believe that crystallization from the melt over such large dimensions, even of arrays of merely microcrystallites, would be thermally reversible at $T = T(\text{room}) = T_g/2$. During the macroscopic melting process all memory of the glassy state is erased and the strain coherence of the transformed region with the substrate is destroyed. There is therefore no remnant driving force (analogous to the mechanical-strain memory field which we have mentioned in our athermal model) which could produce disordering at such low temperatures simply by a thermal process.

There is little doubt that the transformational sequence described here is novel and unexpected. We believe that the thoughtful reader will recognize the inadequacy of the naive melting model as an explanation for the effects we have observed. As we have noted previously,[32] because these laser-induced ordering effects seem to be essentially athermal, the present experiments can be regarded as a paradigm for nonmacroscopic models of laser annealing of other materials[33] such as *a*-Si. Compared to amorphous materials the transformation rates in the present experiment are reduced by a factor of order 10^{12}. This should prove to be very convenient from the point of view of providing a testing ground for liberating our molecular interpretations from the tyranny of macroscopic preconceptions.

Note added in proof. We have recently become aware of studies of laser-induced light absorption oscillations in evaporated $GeSe_2$ films [J. Hajtó and P. Apai, J. Non-Cryst. Solids 35-36, 1085 (1980)]. It appears that many aspects of these oscillations can be connected to the observations reported here. These connections are planned to be discussed elsewhere.

ACKNOWLEDGMENTS

Grateful acknowledgement is made to G. J. Gualtieri and M. Malyj for interfacing the spectrometer with the minicomputer, to M. Malyj for writing all of the software used in data acquisition and analysis, and to A. S. Cooper for some of the x-ray diffraction work.

[1]M. F. Thorpe, in *Vibrational Spectroscopy of Molecular Liquids and Solids,* edited by S. Bratos and R. M. Pick (Plenum, New York, 1979), p. 341.
[2]W. H. Zachariasen, J. Am. Chem. Soc. 54, 3841 (1932).
[3]R. Zahlen, in *Fluctuation Phenomena,* edited by E. W. Montroll and J. L. Lebowitz (North-Holland, Amsterdam, 1979), p. 177.
[4]G. S. Cargill, Ann. N.Y. Acad. Sci. 279, 208 (1976).
[5]F. Betts, A. Bienenstock, and S. R. Ovshinsky, J. Non-Cryst. Solids 4, 554 (1970).
[6]R. J. Bell, N. F. Bird, and P. Dean, Solid State Phys. C1, 299 (1968).
[7]G. Lucovsky, F. L. Galeener, R. C. Keezer, R. H. Geils, and H. A. Six, Phys. Rev. B 10, 5134 (1974).
[8]G. Lucovsky, F. L. Galeener, R. H. Geils, and R. C. Keezer, in *The Structure of Non-Crystalline Materials* edited by P. H. Gaskell (Taylor and Francis, London, 1977), p. 127.
[9]R. J. Nemanich, S. A. Solin, and G. Lucovsky, Solid State Commun. 21, 273 (1977) and references cited therein.
[10]G. Lucovsky, R. J. Nemanich, and F. L. Galeener, in *Proceedings of the VIIth International Conference on Amorphous and Liquid Semiconductors, Edinburgh, 1977,* edited by W. E. Spear (CICL, University of Edinburgh, Edinburgh, 1977), p. 130, and references cited therein.
[11]G. Lucovsky, in *Amorphous Semiconductors,* (edited by M. Brodsky (Springer, New York, 1979), Vol. 36, p. 215.
[12]A. Feltz, K. Zichmuller, and G. Pfaff, in Ref. 10, p. 125.
[13]R. J. Nemanich, G. A. N. Connell, T. M. Hayes, and R. A. Street, Phys. Rev. B 18, 6900 (1978).
[14]R. A. Street, R. J. Nemanich, and G. A. N. Connell,

Phys. Rev. B 18, 6915 (1978).
[15]P. M. Bridenbaugh, G. P. Espinosa, J. E. Griffiths, J. C. Phillips, and J. P. Remeika, Phys. Rev. B 20, 4140 (1979); N. Kumagai, J. Shirafuji, and Y. Inuishi, J. Phys. Soc. Jpn. 42, 1261 (1977).
[16]J. Tauc, in *Optical Properties of Solids* (North-Holland, Amsterdam, 1972), p. 277.
[17]G. I. Kim, N. Kumagai, and J. Shirafuji, J. Non-Cryst. Solids 36, 1047 (1980).
[18]K. Tanaka, J. Non-Cryst. Solids 36, 1023 (1980).
[19]P. H. Fuoss, P. Eisenberger, W. K. Warburton, and A. Bienenstock, Phys. Rev. Lett. 46, 1537 (1981).
[20]W. J. Bresser, P. Boolchand, P. Suranyi, and J. P. de Neufville, Phys. Rev. Lett. 46, 1689 (1981).
[21]G. Dittmar and H. Schaffer, Acta Crystallogr. Sect. B 12, 1188 (1976); 12, 2276 (1976).
[22]J. C. Phillips, J. Non-Cryst. Solids 43, 37 (1981).
[23]V. G. Keramides and W. B. White, J. Am. Ceram. Soc. 57, 22 (1974).
[24]L. Toth, J. Hajto, and G. Zentai, Solid State Commun. 23, 185 (1977).
[25]T. Matsushita and A. Suzuki, Thin Solid Films 58, 413 (1979).
[26]T. Takamori, R. Roy, and G. J. McCarthy, Mater. Res. Bull 5, 529 (1970).
[27]L. Ross and M. Bourgon, Can. J. Chem. 47, 2555 (1969).
[28]S. G. Karbanov, V. P. Zlomanov, and A. V. Novoselova, Vestn. Mosk. Univ. Ser. II Khim 23, 96 (1968), as cited in Ref. 27.
[29]C. H. Chen and K. L. Tai, Appl. Phys. Lett. 37, 1075 (1980) have reported the observation of Se whiskers grown on Ag-photodoped Ge_xSe_{1-x} films. They attribute the whisker growth to compressive stresses present after the sensitization process. Here compressive stress develops during annealing because of contact with the silica container walls.
[30]H. Jones, Rep. Prog. Phys. 36, 1425 (1973).
[31]O. Uemura, Y. Sagara, D. Muno, and T. Satow, J. Non-Cryst. Solids 30, 155 (1978).
[32]J. E. Griffiths, G. P. Espinosa, J. P. Remeika, and J. C. Phillips, Solid State Commun. (in press).
[33]See the recent monograph *Laser and Electron Beam Processing of Materials*, edited by C. W. White and P. J. Peercy (Academic, New York, 1980).